

Lawrence Berkeley National Laboratory

LBL Publications

Title

Rickettsia prowazekii methionine aminopeptidase as a promising target for the development of antibacterial agents

Permalink

<https://escholarship.org/uc/item/7nh0n2pb>

Journal

Bioorganic & Medicinal Chemistry, 25(3)

ISSN

0968-0896

Authors

Helgren, Travis R

Chen, Congling

Wangtrakuldee, Phumvadee

et al.

Publication Date

2017-02-01

DOI

10.1016/j.bmc.2016.11.013

Peer reviewed



HHS Public Access

Author manuscript

Bioorg Med Chem. Author manuscript; available in PMC 2018 February 01.

Published in final edited form as:

Bioorg Med Chem. 2017 February 01; 25(3): 813–824. doi:10.1016/j.bmc.2016.11.013.

***Rickettsia prowazekii* Methionine Aminopeptidase as a Promising Target for the Development of Antibacterial Agents**

Travis R. Helgren[†], Congling Chen[†], Phumvadee Wangtrakuldee[†], Thomas E. Edwards[‡], Bart L. Staker[§], Jan Abendroth[†], Banumathi Sankaran[†], Nicole A. Housley^{||}, Peter J. Myler[§], Jonathon P. Audia^{||}, James R. Horn[†], and Timothy J. Hagen[†]

[†]Department of Chemistry and Biochemistry, Northern Illinois University, 1425 W. Lincoln Hwy, DeKalb, IL 60115, USA

[‡]Beryllium LLC, 7869 NE Day Road West Bainbridge Island, WA 98110, USA

[§]Center for Infectious Disease Research, formerly Seattle Biomedical Research Institute, 307 Westlake Avenue N., Seattle, WA 98109, USA

Seattle Structural Genomics Center for Infectious Disease (SSGCID), Seattle, WA, USA

Department of Global Health and Department of Biomedical Informatics and Medical Education, University of Washington, Seattle, WA 98195, USA

^{||}Berkeley Center for Structural Biology, Ernest Orlando Lawrence Berkeley National Laboratory, Berkeley, CA 94720, USA

^{||}Department of Microbiology and Immunology and The Center for Lung Biology, University of South Alabama College of Medicine, Laboratory of Infectious Diseases, 307 North University Blvd, Mobile, AL 36688, USA

Abstract

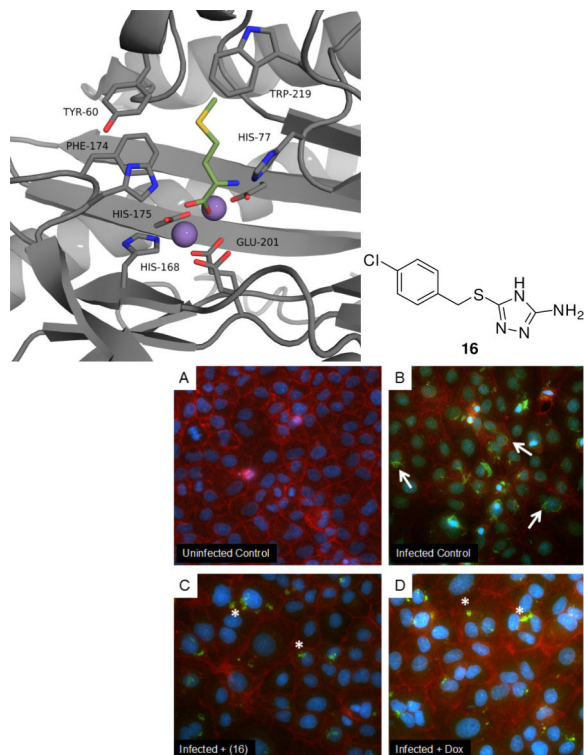
Methionine aminopeptidase (MetAP) is a class of ubiquitous enzymes essential for the survival of numerous bacterial species. These enzymes are responsible for the cleavage of N-terminal *formyl*-methionine initiators from nascent proteins to initiate post-translational modifications that are often essential to proper protein function. Thus, inhibition of MetAP activity has been implicated as a novel antibacterial target. We tested this idea in the present study by targeting the MetAP enzyme in the obligate intracellular pathogen *Rickettsia prowazekii*. We first identified potent *Rp*MetAP inhibitory species by employing an *in vitro* enzymatic activity assay. The molecular docking program AutoDock was then utilized to compare published crystal structures of inhibited MetAP species to docked poses of *Rp*MetAP. Based on these *in silico* and *in vitro* screens, a subset of 23 compounds was tested for inhibition of *R. prowazekii* growth in a pulmonary vascular endothelial cell (EC) culture infection model system. All compounds were tested over concentration ranges that were determined to be non-toxic to the ECs and 10 of the 23 compounds

Correspondence to: Timothy J. Hagen.

Publisher's Disclaimer: This is a PDF file of an unedited manuscript that has been accepted for publication. As a service to our customers we are providing this early version of the manuscript. The manuscript will undergo copyediting, typesetting, and review of the resulting proof before it is published in its final citable form. Please note that during the production process errors may be discovered which could affect the content, and all legal disclaimers that apply to the journal pertain.

displayed substantial inhibition of *R. prowazekii* growth. These data highlight the therapeutic potential for inhibiting *RpMetAP* as a novel antimicrobial strategy and set the stage for future studies in pre-clinical animal models of infection.

Graphical Abstract



Keywords

MetAP; methionine aminopeptidase; inhibition; metalloenzyme; epidemic typhus; *Rickettsia prowazekii*; lung endothelial cells

1. Introduction

Rickettsia prowazekii is an obligate intracytoplasmic pathogen and the causative agent of epidemic typhus fever in humans.^{1,2} Transmission of *R. prowazekii* is mediated by the human body louse and typically associates with deteriorated social conditions resulting in population crowding coupled with compromised sanitation and hygiene.³ These Gram-negative bacteria are vectored via growth in louse gut epithelium and *R. prowazekii* is highly stable when shed in feces, which facilitates the potential for aerosol transmission. *R. prowazekii* is highly virulent,^{4,5} and populations with a low level of immunity are particularly susceptible to this disease.⁶ Patients with typhus exhibit signs and symptoms such as fever, malaise, myalgia, rash, and confusion that are common to numerous diseases, resulting in difficulty in establishing a timely diagnosis.⁷ *R. prowazekii* is designated a select

agent pathogen and classified by the Center for Disease Control and Prevention (CDC) as a category B pathogen and potential bioterrorism agent.⁸

Upon feeding on a human host, the *R. prowazekii*-infected louse defecates at the feeding site and host scratching results in sub-dermal inoculation. Post-inoculation, the rickettsiae ultimately enter the circulation and primarily infect vascular endothelial and immune cells. The rickettsiae attach to a host cell, induce phagocytosis, and rapidly escape the phagolysosome in a phospholipase A₂-dependent manner to grow free in the host cell cytoplasm. *R. prowazekii* typically grows to high numbers in the host cell cytoplasm and are released via host cell lysis to repeat the infection cycle². The obligate intracellular nature of *R. prowazekii* significantly limits the repertoire of clinically effective antibiotic treatments to doxycycline, tetracycline and chloramphenicol. Considering the limited number of antibiotics available to treat rickettsioses and reports of *R. prowazekii* strains resistant to both tetracycline and chloramphenicol,⁹ the identification of novel targets for the development of anti-rickettsial therapeutics is needed.

Nascent bacterial protein synthesis is initiated with an N-terminal *formyl*-methionine residue that may be subsequently removed by the enzymatic activity of methionine aminopeptidases (MetAP) to facilitate proper protein function making this ubiquitous enzyme essential to many bacteria.¹⁰ Previous studies have implicated these enzymes as potentially useful targets for the discovery of novel antibiotics. For example, a nanomolar (IC₅₀) inhibitor of *Burkholderia pseudomallei* MetAP1 was found to exhibit growth inhibition of *B. thailandensis*.¹¹ In the present study, the inhibition activities of three distinct chemical classes of compounds (furoic acids, 1,2,4-triazoles and quinolinols) were evaluated against *R. prowazekii* MetAP1. Structure-activity relationship (SAR) analyses, along with molecular docking, were used to explore potential interactions of these inhibitors within the *Rp*MetAP active site. Finally a subset of 23 inhibitors identified in these *in silico* and *in vitro* screens were tested for inhibition of *R. prowazekii* growth in a cell culture model infection system.

2. Results and Discussion

2.1 Crystal Structures of *Rp*MetAp

The crystal structure of *R. prowazekii* MetAP was solved in two different crystal forms, to 1.7 Å and 2.0 Å resolution. Seven different constructs were designed using structure-based alignments to *Escherichia coli* MetAP (*Ec*MetAP). Constructs varied by small truncations at both the N and C terminus of the *Rp*MetAP sequence of 259 residues (see Supplemental Information, Table S2) as well as 2 full-length constructs with different N-terminal His-tagged extensions, where A and B refer to cleavable and non-cleavable His-tag constructs, respectively. These seven constructs were processed through the Seattle Structural Genomics Center for Infectious Disease (SSGCID) high throughput protein production pipeline concurrently. Constructs A1(1–259), A2(1–247), and A3(1–249) expressed insoluble protein. Constructs B1(1–259), A4(3–259), and A6(3–249) expressed soluble protein, were purified and subjected to crystallization trials. Construct A5(3–247) failed at initial cloning, likely due to technical reasons, and was not pursued further. Given that an N-terminal methionine is added to each sequence during cloning, the only difference between the amino termini of the sequences A1(1–259) and A4(3–259) as well as A3(1–249) and A6(3–249) is

a single threonine residue at position 2 in the wild type sequence. This deletion of one residue led to the production of soluble protein in the A4 and A6 constructs, as compared to the insoluble A1 and A3 constructs.

Constructs A4(residues 3–259) and A6(residues 3–249) both crystallized and diffracted X-rays to high resolution. The structure of construct A4(3–259) bound to methionine and the apo structure of construct A6(3–249) were refined to 1.7 Å and 2.0 Å, respectively, and deposited into the Protein Data Bank (PDB) as 3MX6 and 3MR1. The A4 structure contained two copies of the protein in the asymmetric unit and the A6 construct contained four copies of the protein in the asymmetric unit. The two crystal structures are highly similar with an average root mean squared difference (r.m.s.d.) of only 0.34 Å for C_α atoms. The C-terminal portions of both the A4 and A6 proteins are present in both crystal structures with A4 being ordered through residue Tyr259 and the A6 construct being ordered through Leu249; we note that the numbering scheme used for the crystal structures does not include the N-terminal methionine and thus the above residues are labeled Tyr258 and Leu248.

The overall structural fold of *Rp*MetAP was highly similar to MetAP enzymes from other species ranging from bacteria to human. The root mean squared difference (r.m.s.d.) of the core 250 residue ‘pita bread’ fold between the *R. prowazekii* MetAP as compared to *Pseudomonas aeruginosa* (PDB: 4FO7), *E. coli* (PDB: 1XNZ¹²) and *Homo sapiens* (PDB: 4U1B¹³) was 0.985 Å, 0.711 Å, and 0.865 Å, respectively. For both the A4 and A6 *Rp*MetAP structures, no divalent metal ion was included in the crystallization conditions. Two metal ions were clearly present in the electron density. These features were modeled as Mn(II) ions based off similar structures in the literature as well as proper refinement with *B*-factors similar to those of surrounding protein atoms, octahedral geometry and mean bond distances of 2.1–2.2 Å which are appropriate for Mn(II).¹⁴ The CheckMyMetal server¹⁵ was largely in agreement on metal ion selection, although it suggested copper or cobalt as possible alternatives; however, neither of these metal ions refined with *B*-factors equivalent to those of the surrounding residues. For the A4 structure, an additional electron density feature was present, which modeled well as methionine, a byproduct of the enzymatic activity (PDB: 3MX6, Figure 1). In contrast, the A6 construct crystallized in the presence of phosphate buffer, and a phosphate appears bound to both metal ions; the phosphate ion overlays well with the carboxylate of the bound methionine residue. This phosphate orientation is likely biologically relevant (i.e. reflects the binding mode observed for methionine, Figure 1B) since the enzymatic reaction would proceed through a sp³ hybridized transition state and similar interactions with His78, His176, and Glu202 (His77, His175 and Glu201, respectively in Figure 1) would be expected.

2.2 Compound Syntheses

Various classes of inhibitors have been determined to inhibit MetAP activity, including furoic acids, 1,2,4-triazoles, and quinolinols; compounds of these scaffolds were therefore utilized for our study.¹⁶ It is noteworthy that some compounds based upon the quinolinol scaffold have been identified as pan-assay interference compounds (PAINS)¹⁷ due to both their promiscuous inhibition of metalloenzymes and their ability to form reactive methides. As this is early stage, proof of concept research, this information can be useful in the design of

next generation compounds that are devoid of such characteristics. Importantly, this subset of compounds (**24–26**) do exhibit selective toxicity towards *R. prowazekii* growing within mammalian host cells (see below) and we have therefore included a discussion of their observed activity and SAR.

Regarding our routes to obtain a screening test set, compounds (**1 – 11**) bearing the furoic acid scaffolding were purchased from a commercial source (Sigma Aldrich, St. Louis, MO). The synthesis of the triazole species was previously reported¹¹ (Scheme 1). Briefly, the compounds were synthesized by base promoted addition of substituted benzyl bromides to the 5-amino-4H-1,2,4-triazole-3-thiol starting material. The reactions were carried out under aqueous conditions and afforded product in fair yield (47 – 92%). Regarding the synthesis of oxine Mannich derivatives, the starting materials were suspended in EtOH and heated overnight to afford the desired products in good yield (43 – 95%) (Scheme 2).¹¹

2.3 Enzymatic Activity Assay

2.3.1 Assay Procedure—Following the synthesis of compounds designed to evaluate the SAR of published bacterial MetAP inhibitors, an enzymatic activity assay was used to evaluate inhibition potencies. The assay employed was adopted from published reports,^{11,18} where MetAP activity is monitored as a function of product formation. Utilizing methionyl aminomethylcoumarin (Met-AMC) as the substrate, enzymatic turnover will cleave the peptide bond producing free AMC, a fluorescent compound with emission at 460 nm.

2.3.2 Activity of Furoic Acid Derivatives—Furoic acid based inhibitors of bacterial MetAPs are among the most potent reported in the current literature.¹⁶ Species of this general structure only exhibit potent inhibition of MetAPs containing Mn(II) cofactors, with essentially no activity observed for MetAPs possessing Fe(II), Co(II) or Ni(II) metals.¹⁶ Although this class of inhibitors have demonstrated activity against a number of bacterial MetAPs, including *Mycobacterium tuberculosis*,^{18–19} *B. pseudomallei*,¹¹ *E. coli*,^{12, 20} and *Acinetobacter baumannii*,²¹ there are currently no reports detailing the selectivity of bacterial versus human MetAPs.

Published reports detailing the inhibition of bacterial MetAPs by furoic acids and thiophenic acids^{11–12, 18–21} have suggested the most potent compounds contain small substituents at the ortho (R_1) position. Generally, the compounds bind via bidentate coordination through the carboxylate to one of the active site metals, with one of the oxygen atoms also exhibiting coordination to the other cofactor (PDB: 3MAT).¹² This binding mode results in a competitive mechanism of inhibition where the catalytic site is blocked by inhibitor coordination, effectively eliminating access by substrate.

In the present study, compound (**6**) utilizes a trifluoromethyl substituent at the ortho (R_1) position and was observed to be the most active compound of this chemical series ($IC_{50} = 0.5 \mu M$) (Table 1). Such activity was essentially mirrored by other compounds utilizing substitution at R_1 , namely (**8**), (**10**) and (**11**), with inhibitory values of 0.9, 0.6, and 0.6 μM , respectively. Only one species containing meta (R_2) substitution, 3-methyl derivative (**9**), exhibited greater activity to that of unsubstituted 5-phenyl-2-furoic acid (**4**), with inhibitory values of 26 and 37 μM , respectively. All other 3 and 4 substituted aryl furoic acids were

found to only weakly inhibit enzymatic activity. As with other reports,^{20d} 5-phenyl-2-thiophenic acid (**1**) was found to exhibit weaker activity than that of the corresponding furan ($IC_{50} = 74$ and $37 \mu M$, respectively). It is noteworthy that compound (**6**) exhibited the only Hill slope outlier (2.1 ± 0.1) and also exhibited the most potent inhibitory activity. As the enzyme concentration was fixed at $1 \mu M$, this may reflect the minimum inhibitory concentration detectable by this assay.

2.3.3 Activity of Triazole Derivatives—Species bearing the 1,2,4-triazole scaffold have been shown to inhibit MetAPs from both bacterial^{11, 18–19, 21–22} and human²³ sources. These compounds have been shown to most effectively inhibit MetAPs utilizing Co(II) or Ni(II) cofactors *in vitro*, with weaker activity observed for Mn(II) cofactors.¹⁶ Interestingly, MetAP species bearing Fe(II) cofactors exhibit essentially no reduction in enzymatic turnover in the presence of triazole inhibitors.

Crystal structures detailing the binding of 1,2,4-triazoles to bacterial MetAP targets exist (PDB: 3IU8, 3IU9),¹⁹ where compounds bind via coordination of the 1N and 2N atoms of the triazole ring to the divalent metal cofactors embedded within the active site of MetAPs. Additional binding contacts generally include π - π stacking with aromatic residues (phenylalanine, histidine, and tyrosine) occupying adjacent space to the substrate-binding pocket. A similar binding mechanism is observed for *HsMetAP2*, with coordination to the metal cofactors by the triazole ring and additional π - π stacking to aromatic residues (PDB: 2OAZ).²³

Concerning the inhibition of *RpMetAP* by 1,2,4-triazoles, we determined the most potent compounds utilize electron withdrawing groups (Cl or F) at the R_1 and R_2 position; other reports detailing the inhibition of bacterial MetAPs by this chemical class have confirmed this observation (Table 2).^{18, 21} However, the most potent compound containing benzyl thioethers employed in our study was found to be unsubstituted derivative (**12**) with an IC_{50} value of $6.6 \mu M$, although 2,4-dichloro derivative (**15**) exhibited comparable activity ($IC_{50} = 7.7 \mu M$).

2.3.4 Activity of Quinolinol Derivatives—Compounds composed of the 8-quinolinol scaffold have been screened against MetAPs from *B. pseudomallei*,¹¹ *M. tuberculosis*,²⁴ *E. coli*,²⁵ *Staphylococcus aureus*,^{25c} and against those of human origin.^{25c} The chelating ability of 8-quinolinol derivatives affords an interesting mechanism of binding for metalloenzymes as demonstrated by the crystal structure of an 8-quinolinol derivative bound to *E. coli* MetAP (PDB: 2BB7),^{25b} although the inhibitor is the related compound, 8-quinolinyl-methanesulfonamide. The crystal structure shows the inhibitor binding to a tertiary Mn(II) cofactor found within the active site, and the inhibitor potency was found to be dependent upon the concentration of $MnCl_2$ added to the assay buffer.^{25b} Given the structure-activity relationship previously discovered for the inhibition of *B. pseudomallei*,¹¹ we felt it was appropriate to screen a class of aminoalkylated quinolinol analogues against *R. prowazekii* MetAP.

In our previous study investigating the inhibition of *BpMetAP1*,¹¹ it was found that quinolinol derivatives utilizing NO_2 groups *para* (R_2) to the hydroxyl group exhibited the

most potent activity. Species bearing Cl groups at the same position were essentially inactive. In this study, the opposite appears to be true, with all Cl derivatives being more potent inhibitors than the corresponding NO₂ derivatives. However, the metals employed as cofactors for this study were Mn(II), while Co(II) was used previously in the study of *B. pseudomallei* MetAP inhibitors. This may explain the observed difference in activity regarding Cl or NO₂ substitution, as observed activities have been documented to be highly dependent upon the identity of the metallic cofactors.^{25b}

When compared to aminoalkylated derivatives, unsubstituted quinolinols exhibited superior activity. For example, the most active species was found to be 5-chloro-8-quinolinol (**22**), with an IC₅₀ value of 0.9 μM. All other derivatives (2-methyl-8-quinolinol (**20**), 8-quinolinol (**21**), and nitroxoline (**23**)) exhibited comparable activity to that of (**22**). Concerning aminoalkylated derivatives, all were inferior inhibitors than the corresponding quinolinol fragments.

2.4 Molecular Docking

To discern potential binding interactions and to aid in the development of new MetAP inhibitors, test compounds from each class were docked into the crystal structure of *R. prowazekii* MetAP1 (PDB: 3MX6) and the docking poses and scores were compared to the observed inhibitory data and currently available crystal structures. The docking studies were performed using the open-source program AutoDock.²⁶ The numerous crystal structures of *E. coli* MetAP including substituted 5-aryl-2-furoic acids (PDB: 1XNZ,¹² 2EVM,^{20e} 2Q92,²⁷ 2Q93,²⁷ 2Q94,²⁷ 2Q95,²⁷ 2Q96,²⁷ and 3IU7¹⁹) served as models to validate the docking output from AutoDock (see Supplemental Information). A sequence alignment was performed to discern the conservation between *Ec*MetAP1 and *Rp*MetAP1 (PDB: 1XNZ¹² and 3MX6), which are 53% identical (Figure 2). Based upon the three-dimensional structure, the active site, including the five residues responsible for metal cofactor binding and residues composing the active site surface, is highly conserved.

The crystal structure of the *Ec*MetAP/furoic acid (**10**) complex reveals contacts responsible for potent inhibition (Figure 3B). The most important interactions between the ligand and receptor involve coordination to both the metal cofactors via the carboxylate, π-π interactions with Tyr62 and hydrophobic interactions with His63, Tyr65, His79, Phe177, His178 and Trp221 (Table 4). Additionally, the furoic acid inhibitor exhibits a dihedral angle of 40.6° between the furan and aryl ring. As previously stated, this rotated bi-aryl ring system is necessary for potent inhibition, maximizing interactions with Tyr62. Thus, the incorporation of large substituents at the *ortho* position affords hindered rotation about the bi-aryl axis, resulting in an increase in the dihedral angle, which serves as the basis for the observed increase in activity for this substitution pattern.

The series of furoic acid inhibitors (Table 4) was screened *in silico* against *Rp*MetAP1 to optimize the docking method. Because AutoDock does not automatically assign charges to metal ions, the charge of the Mn(II) cofactors found within the *Rp*MetAP1 structure (3MX6) was manually set at 0.5 elementary charge units (see Supplemental Information). Additionally, compound (**10**) was previously crystallized with *Ec*MetAP1 as a bound

structure (1XNZ),¹² allowing for the comparison of the predicted docking pose and crystal structures for two highly conserved MetAPs of bacterial origin.

The highest scored docking pose of (**10**) reveals a binding mode similar to that observed in the crystal structure of (**10**) bound to *Ec*MetAP1 (Figure 3). As demonstrated in Table 4, the differences in protein-ligand interactions between the crystal and docked structures ranged from 0.1 – 0.9 Å. However, the most obvious difference between the docked and crystal structures is the dihedral angle between the ring systems of the furoic acid inhibitor. The dihedral angle for the docked structure was significantly reduced, at 18°, compared to that of the actual pose (see Supplemental Information). Examination of the Mn-O-Mn bond angle and Mn-O bond distances demonstrates the closer spatial orientation of the inhibitor in the docked pose as compared to that of the actual crystal structure. The large Mn-O-Mn bond angle (155°) and shortening of the chelation distance between the Mn and carboxylate for the docked pose revealed stronger predicted interactions than actually observed (Table 4). The chloride substituent was also found to point into the middle of the substrate binding pocket, rather than coordinate to residues lining the active site as seen in the crystal structure.

2.5 Comparison of *Hs*MetAPs and *Rp*MetAP1

To develop selective inhibitors that target bacterial MetAPs, a detailed understanding of the differences between bacterial and human MetAP structures is necessary. The sequence alignment of *Rp*MetAP1 and *Hs*MetAP1 indicates the enzymes are 43% identical, with all 5 residues responsible for cofactor binding being conserved (Figure 4, bottom). Active site residues were found to be highly conserved, with only a few significant non-conserved residues lining the entrance to the binding pocket (Lys61Tyr, Asp164Ser, Thr166Cys, Ser179Asn, and Leu213Thr, indicating the residue change from *Hs* to *Rp*) as demonstrated by the colored surface model shown in Figure 4. Selective inhibitors will likely utilize binding to the metal cofactors as an anchor for proper binding orientation while targeting interactions with the non-conserved residues. The closest non-conserved residue near the active site of *Rp*MetAP1 is Lys61. Inhibitors have been found to interact with this residue position for *Ec*MetAP1¹² (histidine for the *E. coli* isoform (His63), see Figure 3) and selective inhibition of *Rp*MetAP1 may result from designing inhibitors targeting Lys61. Although docking studies of (**10**) with *Rp*MetAP1 suggests Lys61 lies too far from the active site to allow favorable interactions with bound inhibitors (Table 4), new molecular species could be designed to capitalize upon this lack of conservation and yield selective inhibition.

Of the species screened for *Rp*MetAP1 inhibitory activity (**1** – **26**), compounds bearing the quinolinol scaffold have been evaluated against both *Hs*MetAP1 and *Hs*MetAP2, previously.²⁸ Because *Hs*MetAP1 was determined to be most active with Co(II) cofactors, this metal was employed in the screening of quinolinol compounds in the published report.²⁸ Additionally, Mn(II) has been suggested as the native cofactor for *Hs*MetAp2 and this metal was used in the corresponding assays.^{28–29} In the present study, the compounds exhibit selective inhibition of *Rp*MetAP1 over *Hs*MetAp1, with the compounds generally being inactive against *Hs*MetAp1 (Table 5). This result is interesting, as quinolinol species have

been demonstrated to inhibit MetAP species utilizing Co(II) cofactors over species utilizing Mn(II) cofactors.¹⁶ The quinolinol compounds were not as selective against *HsMetAP2*, with the observed activities being comparable to *RpMetAP1* (Table 5). However, *HsMetAP2* inhibition has been suggested as a treatment for tumor growth abatement (antiangiogenic properties)³⁰ and a lack of specificity regarding these two targets may not be of striking clinical significance.

2.6 Host-Cell Viability Assay

Based on the *in silico* and *in vitro* screens, a subset of 17 *RpMetAP*-inhibitory compounds was selected for testing against *R. prowazekii* growth in a cell culture model infection system (Table 6). Considering that *R. prowazekii* is a vasculotropic pathogen, we used primary pulmonary vascular endothelial cells (ECs) of rat origin for the infection studies. In order to design an assay that was compatible with working under BSL-3 conditions at moderate throughput, our strategy here was to use host cell viability as an indirect measure of rickettsial intracellular growth. Under typical infection conditions, rickettsiae grow inside the host cell to large numbers until the host cell succumbs to infection and lyses. Thus, any *RpMetAP*-inhibitory compound that inhibits rickettsial growth will protect host cell viability over the infection time course. To this end, we used a cell proliferation assay where the amount of water-soluble tetrazolium salt-1 (WST-1) metabolism directly correlates with the number of viable cells.

There are several noteworthy considerations pertaining to rickettsial obligate intracellular growth and our study design. Firstly, rickettsiae are not free-living organisms like *E. coli*. Rickettsiae cannot be grown in pure culture and thus, typical antibiotic resistance screening using, for example, Mueller-Hinton agar and disc diffusion susceptibility assays are not applicable. Secondly, because rickettsiae must grow inside of a eukaryotic host cell, it is not reasonable to design assays based on direct exposure of the pathogen to potential antibiotic compounds. A physiologically relevant screening system must consider the biology of both pathogen and host. This includes diffusion of compounds into the eukaryotic host cell cytoplasm and metabolism/break-down of the compounds by host cell metabolism. Lastly, it is important to note that due to their obligatory intracellular growth consideration of selective toxicity is of paramount importance. Any perturbations that adversely affect host EC health will indirectly result in *R. prowazekii* growth inhibition. Thus, great care was taken to determine the effects of solvents on *R. prowazekii* and EC viability, and to test for off-target effects of the *RpMetAP*-inhibitory compounds on EC viability prior to screening against *R. prowazekii*-infected ECs. We first determined the optimal concentration of solvent (DMSO) used to dissolve the *RpMetAP*-inhibitory compounds that was non-toxic to both the ECs and *R. prowazekii* (optimal concentration was determined to be 0.3% DMSO, data not shown). We next tested the *RpMetAP*-inhibitory compounds over a range of concentrations ranges on uninfected ECs and identified concentration ranges that were non-toxic to the ECs (data not shown). Based on the solubility of the *RpMetAP*-inhibitory compounds in 100% DMSO and the preliminary EC toxicity screen, we selected the optimal concentration ranges for testing each of the 23 *RpMetAP*-inhibitory compounds against *R. prowazekii*-infected ECs (see Table 6).

Figure 5 shows the effects of each of the compounds at the maximal concentration tested. Control, uninfected EC monolayers were healthy and displayed robust WST-1 metabolism (solid black bar labeled U). When EC monolayers were infected with *R. prowazekii* (at an MOI = 100:1), host EC metabolism of WST-1 was reduced 2-fold at 72 hours post-infection (solid grey bar labeled Rp), indicating that *R. prowazekii* intracellular growth reduced host EC viability. This result was confirmed visually under the microscope where monolayers looked stressed with the presence of visible cellular debris (data not shown). The combination of *R. prowazekii* infection and the addition of the solvent control (0.3% DMSO) gave results comparable to infected ECs without DMSO (solid grey bar labeled Rp +DM). The remainder of Figure 5 and Table 6 show 10 promising *RpMetAP*-inhibitory compounds out of the 23 tested that restored *R. prowazekii*-infected EC viability to levels equal to or greater than the uninfected control ECs. The sensitivity of this viability assay was further assessed using EC monolayers infected with a lower burden of rickettsiae (MOI = 50:1), which resulted in only a 1.2-fold reduction in host EC viability, and revealed a similar subset of *RpMetAP*-inhibitory compounds as restorative of host EC viability (data not shown).

When tested serially at 10-, 100- and 1000-fold dilutions, the *RpMetAP*-inhibitory compounds lost inhibitory efficacy indicating that the maximal concentration tested was the most effective at inhibiting *R. prowazekii* growth (data not shown). It is unknown as to whether permeability into the host ECs or compound metabolism/turnover played any role in the observed loss of efficacy. Again, it is noteworthy that inhibitory compounds will only exhibit anti-rickettsial activity via uptake by the host EC cells, followed by uptake by the obligate intracellular parasite cells; this assay therefore mimics practical application better than cases where suspected therapeutics are introduced to free-living pathogens.

Interestingly, the data in Figure 5 show several of the *RpMetAP*-inhibitory compounds stimulated host EC metabolism to levels greater than the control, uninfected and untreated cells. In fact, the preliminary screen of *RpMetAP*-inhibitory compounds for off-target toxicity on uninfected ECs revealed 8 of 23 compounds stimulated host EC metabolism (data not shown). The nature of this metabolic stimulatory effect is unknown. It is noteworthy that of the compounds that stimulated EC metabolism, only 4 were found to also inhibit rickettsial growth (**12,15,16,22**). However, studies with compound (**16**) visually demonstrate rickettsial death upon treatment (Figure 6). Together these data suggest that targeting *R. prowazekii* MetAP is selectively toxic to the rickettsiae and may represent a novel class of anti-rickettsial therapeutics.

The furoic acid inhibitors were the most potent of the classes of compounds screened in the enzymatic assay, but did not restore *R. prowazekii*-infected host cell viability. The results of the host-cell viability assay therefore suggest furoic acid inhibitors are not readily permeable to host ECs, are not permeable to bacteria residing within host ECs, or the native cofactors of *RpMetAP* are not Mn(II). Considering that free carboxylic acids are known to exhibit minimal membrane permeability, the observed lack of anti-rickettsial activity is likely the result of poor cellular uptake.³¹ As such, compounds (**6**) and (**8**) were not screened for host-cell viability, although they exhibited similar activity as compounds (**10**) and (**11**) when screened against *RpMetAP*1.

All quinolinol-based *RpMetAP1* inhibitory compounds were screened in the host-cell viability assay, regardless of the activity observed against the enzyme, because all but two compounds, (**25** – **26**), exhibited IC₅₀ values less than 10 μM. Interestingly, three compounds from this chemical class were determined to restore *R. prowazekii*-infected host cell viability. Two were unsubstituted 8-quinolinol derivatives (**21**, **22**) while the remaining compound (**26**) was a Mannich derivative of nitroxoline (**23**).

The most effective compounds for restoring host-cell viability were from the 1,2,4-triazole series. Because these compounds were determined to exhibit similar inhibitory activities against the *RpMetAP1* target, all eight analogs from this series were tested and five exhibited anti-rickettsial activity (**12** – **16**) while restoring host-cell viability. The three analogs (**17** – **19**) that did not restore host-cell viability contained lipophilic substituents that increased their cLogP values and lowered their solubility.

Finally, we assayed compound (**16**), which both inhibited *RpMetAP1* activity and stimulated host EC metabolism, to investigate whether the compound inhibited rickettsial growth by fluorescence staining and microscopy to provide a visual representation of the observed effects. For these experiments, doxycycline was included as a clinically relevant positive control to inhibit rickettsial intracellular growth. Figure 6A shows a healthy, uninfected and untreated control EC monolayer with Hoechst-stained nuclei (blue pseudocolor) and phalloidin-stained actin outlining cell boundaries (red pseudocolor). Figure 6B shows the presence of several host ECs infected with intracellular, rod shaped *R. prowazekii* stained with an anti-rickettsial antibody (green pseudocolor). Figure 6C shows treatment of infected host ECs with compound (**16**) resulted in identification of intracellular debris that stained with the anti-rickettsial antibody but did not resemble healthy, rod-shaped bacteria shown in Figure 6B; this data strongly suggests that intracellular rickettsial growth abatement had occurred. We confirmed visually that addition of compound (**16**) alone had no overt effect on the appearance of the monolayers (data not shown). Moreover, a similar pattern of staining with the anti-rickettsial antibody was also observed when infected ECs were treated with doxycycline as a positive control known to inhibit rickettsial growth (Figure 6D). Together, these results confirm the promise of compound (**16**) as representative of a novel class of anti-rickettsial therapeutics that do not appear to have overt deleterious effects on host EC ultrastructure by fluorescence staining and microscopy.

3. Conclusions

A series of compounds based upon furoic acid, 1,2,4-triazole, and quinolinol motifs were synthesized or purchased and screened for enzymatic inhibitory activity against *R. prowazekii* MetAP. Suspected *RpMetAP1* inhibitory compounds were first screened against the enzyme in a fluorescence-based activity assay, with Mn(II) utilized as the enzymatic cofactors. It was determined that compounds based upon all three scaffolds exhibited potent inhibitory activity. The most active compounds were subjected to a host cell viability assay to determine anti-*Rickettsial* activity in the presence of host endothelial cells, which revealed only quinolinol and triazole-based inhibitors were active at “reasonable” concentrations. The lack of observed activity from the furoic acid series may be due to limited membrane permeability of small molecules containing free acid groups. The most potent compound in

the host-cell viability assay was 2-chlorophenyl 1,2,4-triazole derivative (**16**) and the activity of this compound was therefore monitored with fluorescence staining and microscopy to provide a visual representation of the anti-*Rickettsial* activity in the presence of mammalian host-cells. These data suggest that compounds based upon both the 1,2,4-triazole and quinolinol scaffolds exhibit efficacy against the intracellular pathogen while allowing the restoration of host-cell viability. Thus, compounds of these classes should be optimized against *RpMetAP1* and the resulting species should be re-screened to determine anti-*Rickettsial* activity in the presence of mammalian host-cells.

4. Experimental

4.1 Crystallization and Data Collection

Purified *RpMetAPs* were screened for crystallization in 96-well sitting-drop plates against the JCSG+ and PACT crystal screens (Rigaku Reagents). Equal volumes of protein solution (0.4 μ l) and precipitant solution were set up at 293 K against reservoir (80 μ l) in sitting-drop vapor-diffusion format. The A4 construct crystallized in the PACT screen condition G8 which contains 0.2 M sodium sulfate, 0.1 M BisTris propane pH 7.5, and 20% w/v PEG 3350. The A6 construct crystallized in the PACT screen condition A6 which contains 0.1 M SPG (succinic acid, phosphate, glycine) buffer pH 8.0 and 25% w/v PEG 1500. The crystals were cryo-protected in crystallant plus 25% v/v 1,2-ethanediol and cryo-cooled by dipping into liquid nitrogen. Data were collected under the Collaborative Crystallography program of the Berkeley Center for Structural Biology at the Advanced Light Source, Berkeley National Laboratory. Data were collected at 100 °C on Advanced Light Source beamline 5.0.1 using an ADSC Quantum 315 CCD detector with 1° oscillations at a wavelength of 0.9774 Å. Data were reduced with HKL2000³². Raw X-ray diffraction images are available at the Integrated Resource for Reproducibility in Macromolecular Crystallography at www.proteindiffraction.org.

4.2 Structure Solution and Refinement

The structure was solved by molecular replacement with Phaser from the CCP4 suite of programs using PDB entry 1XNZ¹² as a search model.³³ The structure was refined using iterative cycles of Refmac5 followed by manual rebuilding of the structure using Coot.³⁴ The quality of all of the structures was assessed using MolProbity.³⁵ All data-reduction, refinement, and data collection statistics can be found in Table S3. Structure figures were analyzed and prepared using PyMOL (v.1.5; Schrodinger) and PISA. Coordinates and structure factors have been deposited with the Protein Data Bank (PDB) (<http://www.rcsb.org/pdb/home/home.do>) with accession number 3MR1 and 3MX6.

4.3 *RpMetAP* Cloning and Purification

Cloning, expression and purification were conducted as part of the Seattle Structural Genomics Center for Infectious Disease (SSGCID) following standard protocols described previously.³⁶ All constructs of *RpMetAP* (Uniprot: Q9ZCD3) were PCR-amplified from *Rickettsia prowazekii* str. Madrid E kindly provided by Dr. David H. Walker. A full length (1-259) and five variant open reading frames (ORF) were cloned into the ligation independent cloning (LIC) expression vector pAVA0421 encoding a cleavable 6xHis fusion

tag followed by the human rhinovirus 3C protease-cleavage sequence (MAHHHHHHMGTLEAQTQGPGSM) followed by the ORF.³⁷ The human rhinovirus 3C protease-cleavage site is between the glutamine and glycine residues that are underlined. An additional full length construct was cloned into the expression vector pBG1861 which encodes a non-cleavable 6xHis fusion tag (MAHHHHHH). See Supplemental Information, Table S2 for list of constructs. Complete amino acid sequences are included in supplementary materials.

Plasmid DNA was transformed into chemically competent *E. coli* BL21 (DE3) R3 Rosetta cells. Cells were expression tested in 96 well blocks according to the procedures described in Choi, et al., 2011.^{36e} Briefly, cells are inoculated into 600 μ l ZYP-5052 auto-induction medium [Sterile ZY Broth (10 g/L tryptone, 5 g/L yeast extract), 1 mM MgSO₄, 1 \times metals mix, 1 \times 5052 (0.5% glycerol, 0.05% glucose, 0.2% α -lactose monohydrate) and 1 \times NPS] supplemented with the correct antibiotics. The block was sealed and incubated on a plate shaker inside a refrigerated incubator set at 293 K for roughly 27 h to allow the cultures to reach saturation or early stationary phase. The cultures were not harvested until OD_{600nm} readings of at least 0.6 were obtained. Once the induced cells were at the correct density, they were centrifuged at 4 °C and 4300 rpm for 30 min. After centrifugation, the supernatant was discarded and the block with the semi-dry cell pellets were stored at 193 K. Cell pellets were analyzed for expression of insoluble and soluble RpMetAP by re-suspension in 600 μ l lysis buffer [20 mM HEPES pH 7.0, 500 mM NaCl, 5% glycerol, 0.5% CHAPS (A.G. Scientific Inc., San Diego, California, USA), 30 mM imidazole, 10 mM MgCl₂, 400 μ g ml⁻¹ lysozyme (Sigma, St Louis, Missouri, USA) and 3 units/mL Benzonase nuclease (EMD Chemicals, San Diego, California, USA). After resuspension, 600 μ l lysis buffer was added to each well and the sample was mixed a second time. The deep well block was then sealed and incubated at room temperature for 1 h on a titer shaker set to moderate. The block was clarified by centrifugation at 4300 rev min⁻¹ for 30 min. Soluble and insoluble fractions were analyzed by SDS-PAGE for bands of appropriate MW. Only RpMetAP constructs which showed soluble expressed protein progressed into further large scale fermentation and purification. Constructs B1, A4 and A6 (see Table S2) expressed soluble protein and were further upscaled and purified by IMAC and Size exclusion chromatography (SEC) as described previously.^{36e} Proteins were concentrated and stored in the final SEC running buffer was composed of 20mM HEPES pH 7, 0.3M NaCl, 5% glycerol, 1mM TCEP. Aliquots of 100 μ l were cryo-cooled in liquid nitrogen and stored at -80 °C until use for crystallization.

4.4 Enzymatic Assay

The assay utilized is similar to that which we reported earlier.^{11,18} The fluorogenic peptide substrate, methionine-aminomethylcoumarin was purchased from Enzo Life Sciences (Farmingdale, NY). Purified RpMetAP1a was obtained from the Seattle Structural Genomics Center for Infectious Disease (SSGCID) and was used as received. Enzyme stock solutions were prepared by diluting RpMetAP1a into assay buffer (6.25 mM HEPES, 0.1 mM MnCl₂, 125 mM NaCl, pH 7.0) and adjusting enzyme concentration to 4 μ M, where concentration was determined from solution absorbance at 250 nm (measured with a Thermo Scientific NanoDrop 2000c, extinction coefficient = 30,370 M⁻¹ cm⁻¹). Enzymatic

activity of *RpMetAP* was followed using a Synergy 2 Plate reader (Biotek, Winooski, Vt). All kinetic experiments were performed using Nunc flat-bottom maxisorp 96-well plates (Thermo Fisher Scientific, Rochester, NY). Each well contained 80 μ L of assay mixture with final concentrations of 6.25 mM HEPES, 0.1 mM $MnCl_2$, 125 mM NaCl, 200 μ M Met-AMC, 1.0 μ M *RpMetAP*1, and 1% DMSO at pH 7.0 and at various inhibitor concentrations. First, enzyme from prepared stock solutions (20 μ L) and inhibitors at variable concentrations (20 μ L, 4% DMSO) in assay buffer was centrifuged (4 $^{\circ}$ C, 2000 rpm, 5 min) and incubated for 1 h at 4 $^{\circ}$ C. Then, substrate (40 μ L, 400 μ M) in assay buffer was added to each well, centrifuged (4 $^{\circ}$ C, 2000 rpm, 5 min), and incubated at 30 $^{\circ}$ C in the plate reader for 30 min. The fluorescent emission resulting from the cleavage of Met-AMC was monitored for 90 min (Excite: 360 nm, Read: 460 nm). Relative activities of enzyme/substrate solutions were determined as the slope of inhibited enzyme divided by the slope of free enzyme. The first 30 min of data were discarded as this was considered condition equilibration. Inhibitory activities were calculated as the ratio of inhibited and uninhibited enzyme activity (v_i / v_o) and dose-response curves were fit according to published methods.³⁸

4.5 Molecular Docking

Detailed information regarding the validation of this docking method can be found in the supplemental information submitted with this manuscript. Briefly, ligand structures were composed in ChemDraw and the minimum energy conformation was calculated with Chem3D. These were used as the initial ligand conformations for docking. Grid box dimensions were (50,50,50) and were centered between the metal cofactors for both structures (coordinates (x,y,z): *EcMetAP*: (2.258, 0.561, 9.365); *RpMetAP*: (11.561, -12.202, 9.441)). Docking output was evaluated based upon both the predicted docking poses and predicted binding affinities (K_i).

4.6 *R. prowazekii* Infection of Cultured Pulmonary Vascular Endothelial Cells and Treatment with *RpMetAP* Inhibitory Compounds

All infection experiments described in this study used the virulent *R. prowazekii* strain Breinl propagated in and isolated from hen egg yolk sacs (Audia laboratory passage #3) as previously described³⁹ with the modifications described in.⁴⁰ Post-isolation, *R. prowazekii* were suspended in a solution consisting of 220 mM sucrose, 12 mM potassium phosphate, 4.9 mM potassium glutamate, and 10 mM magnesium chloride, pH 7.0 (SPGMg²⁺) and stored as frozen aliquots at -80 $^{\circ}$ C until used. Post-thaw on ice, total infectious organisms per mL of suspension were determined using the modified hemolysis assay of Winkler and Walker,⁴¹ which was subsequently used to calculate experimental multiplicities of infection (MOI). All manipulations of infectious *R. prowazekii* were performed under BSL-3 conditions.

Primary pulmonary vascular endothelial cells (ECs) of CD rat origin were isolated and characterized as previously described.⁴² For the studies described here, cultured ECs of low passage number (< 15) were kindly provided by the University of South Alabama Center for Lung Biology Cell Culture Core. ECs were routinely cultured as adherent monolayers in plastic culture dishes (at 37 $^{\circ}$ C, 5% CO₂, atm O₂) in DMEM high glucose medium (without phenol red) supplemented with 10% fetal bovine serum and 4 mM L-glutamine (DMEM/

FBS). For all experiments, ECs suspended in DMEM/FBS were stained with erythrosin B (0.025% final concentration) and enumerated in a Fuchs-Rosenthal counting chamber prior to seeding.

To prepare ECs for infection, 2.5×10^4 total ECs (per 0.1 mL DMEM/FBS) were seeded in 96-well culture plates and incubated overnight to allow for adherence and monolayer formation (~18 hours, at 37 °C, 5% CO₂, atm O₂). A frozen aliquot of *R. prowazekii* was thawed on ice, diluted in DMEM/FBS to give a concentration of infectious rickettsiae per 0.1 mL equivalent to a MOI of either 100 rickettsiae per host cell (100:1) or 50 rickettsia per cell (50:1). The DMEM/FBS seeding medium was removed from each well and replaced with 0.1 mL of rickettsiae-containing medium to initiate infection. Control, uninfected wells received only DMEM/FBS. Culture plates were then returned to the incubator (at 37 °C, 5% CO₂, atm O₂).

At 24-hours post-infection the culture medium was removed from each well and replaced with 0.1 mL of: 1) DMEM/FBS only (control), 2) DMEM/FBS containing 0.3% DMSO (*RpMetAP* inhibitory compound solvent/vehicle control), or 3) DMEM/FBS containing *RpMetAP* inhibitory compounds (see Table 6 and Results and Discussion section for concentrations tested). Culture plates were returned to the incubator (37 °C, 5% CO₂, atm O₂). All conditions were tested in triplicate and monolayers were visually inspected by light microscopy every 18–20-hours subsequently.

At 72-hours post-infection (corresponding to 48-hours post-compound addition), host EC viability was determined using Roche's WST-1 cell proliferation reagent. A ratio of 1 mL WST-1 reagent was added per 10 mL DMEM/FBS medium (now DMEM/FBS+WST-1) and mixed thoroughly by pipetting. Culture medium was removed from each well and replaced with 0.11 mL of DMEM/FBS+WST-1. Culture plates were returned to the incubator for 60-minutes (at 37 °C, 5% CO₂, atm O₂). A volume of 0.015 mL of 37% formaldehyde solution was added to each well to stop the WST-1 reaction and fix-kill the rickettsiae. We verified that the addition of formaldehyde did not adversely affect the WST-1 signal compared to wells that were not formaldehyde-treated (data not shown). Culture plates were returned to the incubator for an additional 20-minutes (at 37 °C, 5% CO₂, atm O₂). The amount of WST-1 metabolism was determined as per the manufacturer's directions using a microplate reader and medium only wells (with no cells) were also included on the culture plate for background subtraction. Data were plotted as the mean normalized WST-1 signal \pm standard deviation.

4.7 Assessment of *R. prowazekii* Growth Inhibition by Compound (16) Using Fluorescent Microscopy

In order to provide a visual account of the effects of *RpMetAP* inhibitory compounds on *R. prowazekii* intracellular growth, a separate set of infection experiments were performed and slides prepared for staining and fluorescent microscopic analysis. To prepare ECs for infection, 2.5×10^4 total ECs (per 0.2 mL DMEM/FBS) were seeded in 8-well glass chamber slides and incubated overnight to allow adherence and monolayer formation (~18 hours, at 37 °C, 5% CO₂, atm O₂). As described above, ECs were subsequently mock-infected (DMEM/FBS only) or infected with *R. prowazekii* (MOI 50:1) and chamber slides

returned to the incubator (at 37 °C, 5% CO₂, atm O₂). Note that infections were adjusted to a 0.2 mL final volume.

At 24-hours post-infection the culture medium was removed from each chamber well and replaced with 0.2 mL of: 1) DMEM/FBS only (control), 2) DMEM/FBS containing 300 µM compound (**16**), or 3) DMEM/FBS containing 25 µg/mL doxycycline (positive control). All conditions were tested in duplicate. Chamber slides were returned to the incubator (37 °C, 5% CO₂, atm O₂).

At 72-hours post-infection the culture medium was removed from each chamber well and replaced with 0.3 mL of fixative solution (phosphate buffered saline, pH 7.4 [PBS] containing 2.5% formaldehyde). Chamber slides were kept in the biosafety cabinet under ambient conditions for 20-minutes to allow fixation to occur.

To prepare slides for staining, fixative solution was removed and chamber wells were washed once with 0.3 mL PBS. The PBS was discarded, 0.1 mL of blocking solution (PBS containing 0.2% Triton X-100, 10% normal goat serum) added, and chamber slides incubated for 20-minutes under ambient conditions. The blocking solution was discarded, 0.1 mL of staining solution (blocking solution containing 1 µg/mL Hoescht 33258, 0.2 U Texas Red labeled phalloidin, 1:2000 dilution of a FITC-labeled antibody specific to *R. prowazekii*) added, and chamber slides incubated for 45-minutes under ambient conditions (foil wrapped). The staining solution was discarded and slides were washed twice in 0.3 mL of PBS followed by a single wash in 0.3 mL dH₂O. Chambers were removed from the slide, a large glass coverslip (50 mm) was mounted using Invitrogen's Prolong AntiFade medium as per the manufacturer's directions, and slides were allowed to cure overnight under ambient conditions (foil wrapped). Individual images for each fluorescent compound within the same field of view were captured using a Nikon Eclipse Ni microscope with Nikon Elements software. Individual images were overlaid, converted to pseudocolor and brightness and contrast adjusted using Adobe Photoshop. Hoescht-stained nuclei are pseudocolored blue, phalloidin-stained actin cytoskeleton is pseudocolored red and intracellular rickettsiae are pseudocolored green.

Supplementary Material

Refer to Web version on PubMed Central for supplementary material.

Acknowledgments

This project has been funded in part with Federal funds from the National Institute of Allergy and Infectious Diseases, National Institutes of Health, Department of Health and Human Services, under Contract Nos. HHSN272200700057C and HHSN272201200025C. The Berkeley Center for Structural Biology is supported in part by the National Institutes of Health, National Institute of General Medical Sciences, and the Howard Hughes Medical Institute. The Advanced Light Source is supported by the Director, Office of Science, Office of Basic Energy Sciences, of the U.S. Department of Energy under Contract No. DE-AC02-05CH11231. Finally, the authors would like to acknowledge funding from the NIH for construction of the BSL-3 facility at the University of South Alabama (Contract No. C06 RR029870) and for the procurement of a microscope utilized in this study (Contract No. K22 AI089786).

References

1. Bechah Y, Capo C, Raoult D, Mege JL. *J. Infect. Dis.* 2008; 197:142. [PubMed: 18171297]
2. Audia, JP. *Intracellular Pathogens II: Rickettsiales*. American Society of Microbiology; 2012. *Rickettsial Physiology and Metabolism in the Face of Reductive Evolution*.
3. (a) Andersson JO, Andersson SGE. *Res. Microbiol.* 2000; 151:143. [PubMed: 10865960] (b) Raoult D, Woodward T, Dumler JS. *Infect. Dis. Clin. North Am.* 2004; 18:127. [PubMed: 15081509]
4. Zhu Y, Fournier PE, Ogata H, Raoult D. *J. Clin. Microbiol.* 2005; 43:4708. [PubMed: 16145131]
5. Birg ML, La Scola B, Roux V, Brouqui P, Raoult D. *J. Clin. Microbiol.* 1999; 37:3722. [PubMed: 10523584]
6. Walker DH. *Ann. N. U. Acad. Sci.* 2003; 990:739.
7. Walker DH. *Clin. Infect. Dis.* 2007; 45:S39. [PubMed: 17582568]
8. Walker DH. *Vaccine.* 2009; 27:D52. [PubMed: 19837287]
9. Weiss E, Dressler HR. *J. Bacteriol.* 1962; 83:409. [PubMed: 14040210]
10. Chang SY, McGary EC, Chang S. *J. Bacteriol.* 1989; 171:4071. [PubMed: 2544569]
11. Wangtrakuldee P, Byrd MS, Campos CG, Henderson MW, Zhang Z, Clare M, Masoudi A, Myler PJ, Horn JR, Cotter PA, Hagen TJ. *ACS Med. Chem. Lett.* 2013; 4:699.
12. Ye QZ, Xie SX, Huang M, Huang WJ, Lu JP, Ma ZQ. *J. Am. Chem. Soc.* 2004; 126:13940. [PubMed: 15506752]
13. Arya T, Reddi R, Kishor C, Ganji RJ, Bhukya S, Gumpena R, McGowan S, Drag M, Addlagatta A. *J. Med. Chem.* 2015; 58:2350. [PubMed: 25699713]
14. Zheng H, Chruszcz M, Lasota P, Lebioda L, Minor W. *J. Inorg. Biochem.* 2008; 102:1765. [PubMed: 18614239]
15. Zheng H, Chordia MD, Cooper DR, Chruszcz M, Müller P, Sheldrick GM, Minor W. *Nat. Protoc.* 2014; 9:156. [PubMed: 24356774]
16. Helgren TR, Wangtrakuldee P, Staker BL, Hagen TJ. *Curr. Top. Med. Chem.* 2016; 16:397. [PubMed: 26268344]
17. (a) Baell JB, Holloway GA. *J. Med. Chem.* 2010; 53:2719. [PubMed: 20131845] (b) Baell JB. *J. Nat. Prod.* 2016; 79:616. [PubMed: 26900761] (c) Baell JBW, Michael A. *Nature.* 2014; 513:481. [PubMed: 25254460]
18. Lu JP, Ye Q-Z. *Bioorg. Med. Chem. Lett.* 2010; 20:2776. [PubMed: 20363127]
19. Lu JP, Chai SC, Ye Q-Z. *J. Med. Chem.* 2010; 53:1329. [PubMed: 20038112]
20. (a) Chai SC, Ye QZ. *Bioorg. Med. Chem. Lett.* 2010; 20:2129. [PubMed: 20207144] (b) Huang QQ, Huang M, Nan FJ, Ye QZ. *Bioorg. Med. Chem. Lett.* 2005; 15:5386. [PubMed: 16219464] (c) Huguet F, Melet A, Alves de Sousa R, Lieutaud A, Chevalier J, Maigre L, Deschamps P, Tomas A, Leulliot N, Pages JM, Artaud I. *ChemMedChem.* 2012; 7:1020. [PubMed: 22489069] (d) Vedantham P, Guerra JM, Schoenen F, Huang M, Gor PJ, Georg GI, Wang JL, Neuenswander B, Lushington GH, Mitscher LA, Ye QZ, Hanson PR. *J. Combi. Chem.* 2008; 10:185. (e) Xie SX, Huang WJ, Ma ZQ, Huang M, Hanzlik RP, Ye QZ. *Acta Crystallogr. Sect. D.* 2006; 62:425. [PubMed: 16552144] (f) Huang M, Xie SX, Ma ZQ, Huang QQ, Nan FJ, Ye QZ. *J. Med. Chem.* 2007; 50:5735. [PubMed: 17948983] (g) Chai SC, Wang WL, Ye QZ. *J. Biol. Chem.* 2008; 283:26879. [PubMed: 18669631]
21. Yuan H, Chai SC, Lam CK, Howard Xu H, Ye QZ. *Bioorg. Med. Chem. Lett.* 2011; 21:3395. [PubMed: 21524572]
22. (a) Mitra S, Sheppard G, Wang J, Bennett B, Holz R. *J. Biol. Inorg. Chem.* 2009; 14:573. [PubMed: 19198897] (b) Oefner C, Douangamath A, D'Arcy A, Häfeli S, Mareque D, Mac Sweeney A, Padilla J, Pierau S, Schulz H, Thormann M, Wadman S, Dale GE. *J. Mol. Biol.* 2003; 332:13–21. [PubMed: 12946343]
23. Marino JP, Fisher PW, Hofmann GA, Kirkpatrick RB, Janson CA, Johnson RK, Ma C, Mattern M, Meek TD, Ryan MD, Schulz C, Smith WW, Tew DG, Tomazek TA, Veber DF, Xiong WC, Yamamoto Y, Yamashita K, Yang G, Thompson SK. *J. Med. Chem.* 2007; 50:3777. [PubMed: 17636946]

24. Olaleye O, Raghunand TR, Bhat S, Chong C, Gu P, Zhou J, Zhang Y, Bishai WR, Liu JO. *Tuberculosis*. 2011; 91:S61. [PubMed: 22115541]
25. (a) Chai SC, Ye QZ. *Bioorg. Med. Chem. Lett.* 2009; 19:6862. [PubMed: 19889537] (b) Huang M, Xie SX, Ma ZQ, Hanzlik RP, Ye QZ. *Biochem. Biophys. Res. Commun.* 2006; 339:506. [PubMed: 16300729] (c) Altmeyer MA, Marschner A, Schiffmann R, Klein CD. *Bioorg. Med. Chem. Lett.* 2010; 20:4038. [PubMed: 20621724]
26. Morris GM, Huey R, Lindstrom W, Sanner MF, Belew RK, Goodsell DS, Olson AJ. *J. Comput. Chem.* 2009; 30:2785. [PubMed: 19399780]
27. Ma ZQ, Xie SX, Huang QQ, Nan FJ, Hurley TD, Ye QZ. *BMC Struct. Biol.* 2007; 7:1. [PubMed: 17201922]
28. Bhat S, Shim JS, Zhang F, Chong CR, Liu JO. *Org. Biomol. Chem.* 2012; 10:2979. [PubMed: 22391578]
29. Wang J, Sheppard GS, Lou P, Kawai M, Park C, Egan DA, Schneider A, Bouska J, Lesniewski R, Henkin J. *Biochemistry*. 2003; 42:5035. [PubMed: 12718546]
30. (a) Sato Y. *Biol. Pharm. Bull.* 2004; 27:772. [PubMed: 15187415] (b) Benny O, Fainaru O, Adini A, Cassiola F, Bazinet L, Adini I, Pravda E, Nahmias Y, Koirala S, Corfas G, D'Amato RJ, Folkman J. *Nat. Biotech.* 2008; 26:799.
31. Ballatore C, Huryn DM, Smith AB. *ChemMedChem*. 2013; 8:385. [PubMed: 23361977]
32. Otwinowski, Z., Minor, W. *Processing of X-ray diffraction data collected in oscillation mode*. Vol. 276. Elsevier; 1997. p. 307-326.
33. (a) McCoy AJ, Grosse-Kunstleve RW, Adams PD, Winn MD, Storoni LC, Read RJ. *J. Appl. Crystallogr.* 2007; 40:658. [PubMed: 19461840] (b) Winn MD, Ballard CC, Cowtan KD, Dodson EJ, Emsley P, Evans PR, Keegan RM, Krissinel EB, Leslie AGW, McCoy A, McNicholas SJ, Murshudov GN, Pannu NS, Potterton EA, Powell HR, Read RJ, Vagin A, Wilson KS. *Acta Crystallogr. Sect. D*. 2011; 67:235. [PubMed: 21460441]
34. (a) Vagin AA, Steiner RA, Lebedev AA, Potterton L, McNicholas S, Long F, Murshudov GN. *Acta. Crystallogr. Sect. D*. 2004; 60:2184. [PubMed: 15572771] (b) Emsley P, Lohkamp B, Scott WG, Cowtan K. *Acta Crystallogr. Sect. D*. 2010; 66:486. [PubMed: 20383002]
35. Chen VB, Arendall WB, Headd JJ, Keedy DA, Immormino RM, Kapral GJ, Murray LW, Richardson JS, Richardson DC. *Acta Crystallogr. Sect. D*. 2010; 66:12. [PubMed: 20057044]
36. (a) Myler PJ, Stacy R, Stewart L, Staker BL, Van Voorhis WC, Varani G, Buchko GW. *Infect. Disord. Drug. Targets*. 2009; 9:493. [PubMed: 19594426] (b) Stacy R, Begley DW, Phan I, Staker BL, Van Voorhis WC, Varani G, Buchko GW, Stewart LJ, Myler PJ. *Acta Crystallogr. Sect. D*. 2011; 67:979. (c) Serbzhinskiy DA, Clifton MC, Sankaran B, Staker BL, Edwards TE, Myler PJ. *Acta Crystallogr. Sect. F*. 2015; 71:594. (d) Bryan CM, Bhandari J, Napuli AJ, Leibly DJ, Choi R, Kelley A, Van Voorhis WC, Edwards TE, Stewart LJ. *Acta Crystallogr. Sect. F*. 2011; 67:1010. (e) Choi R, Kelley A, Leibly D, Nakazawa Hewitt S, Napuli A, Van Voorhis W. *Acta. Crystallogr. Sect. F*. 2011; 67:998.
37. Aslanidis C, de Jong PJ. *Nucleic Acids. Res.* 1990; 18:6069. [PubMed: 2235490]
38. Grant SK, Sklar JG, Cummings RT. *J. Biomol. Screen.* 2002; 7:531. [PubMed: 14599351]
39. Bovarnick MR, Snyder JC. *J. Exp. Med.* 1949; 89:561. [PubMed: 18129859]
40. Winkler HH. *Infect. Immun.* 1974; 9:119. [PubMed: 4357933]
41. Walker TS, Winkler HH. *J. Clin. Microbiol.* 1979; 9:645. [PubMed: 113426]
42. King J, Hamil T, Creighton J, Wu S, Bhat P, McDonald F, Stevens T. *Microvasc. Res.* 2004; 67:139. [PubMed: 15020205]

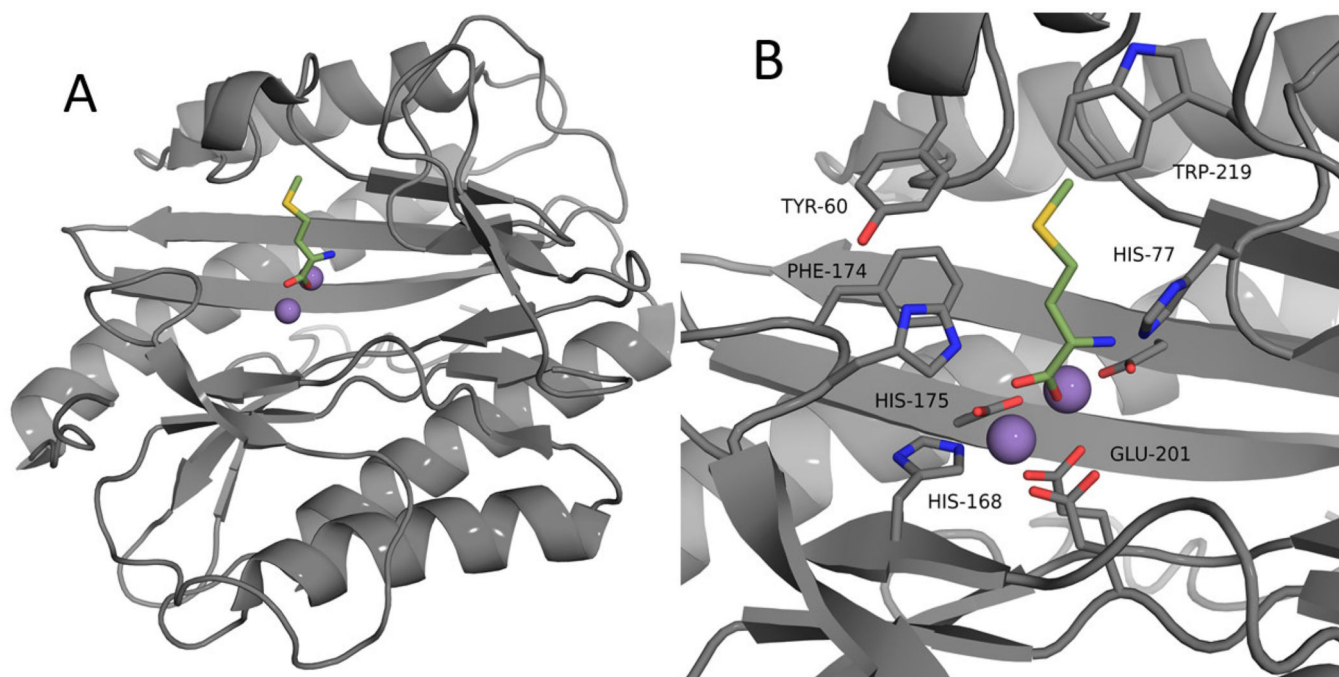


Figure 1.
RpMetAP1 (PDB: 3MX6) with bound methionine. **A:** *RpMetAP* represented as a cartoon.
B: Zoom-in of the *RpMetAP* active site. Purple spheres designate Mn(II) cofactors and the green residue is the bound methionine.


```

EcMetAP 1  ---MAISIKTPEDI EKMRVAGRLAAEVLEMIEPYVKPGVSTGELDRICNDYIVNEQHAVS
RpMetAP 1  GPGSMIKIHTTEKDFIKMRAAGKLAETLDFITDHWKPNVTTNSLNDLCHN-FITSHNAIP

EcMetAP 58  ACLGYHGYPKSVCTISINEVVCHGIPDDAKLLKDGDIVNIDVTVIKDGFGDTSKMFTVVGK
RpMetAP 60  APLNYKGFPKSICTSINHVVCHGIPND-KPLKNGDIVNIDVTVILDGWYGDTSRMYVVD

EcMetAP 118 PTIMGERLCRITQESLYLALRMVKPGINLREIGAAIQKFEVEAEGFSVVREYCGHGIGRGF
RpMetAP 119 VAIKPKRLIQVTYDAMMKGIEVVRPGAKLGDIGYAIQSYAEKHNYSVVRDYTGHGIGRVE

EcMetAP 178  HEEPQVLHYDSRETNVVLKPGMTFTIEPMVNAGKKE-IRTMKDGWTVKTKDRSLSAQYEH
RpMetAP 179  HDKPSILNYGRNGTGLTLKEGMFFTVEPMINAGNYDTILSKLDGWTVTTRDKSLSAQFEH

EcMetAP 237  TIVVTDNGCEILTL--RKDDTIPAIISHDE
RpMetAP 239  TIGVTKDGFEIFTLSPKKLDYPPY-----

```

Figure 2.

Sequence alignment of *EcMetAP1* (PDB: 1XNZ)¹² and *RpMetAP1* (PDB: 3MX6) shaded according to alignment (dark = identity; light = similarity; no shading = non-conserved).

Alignment reveals 53% identity between the proteins. Residues involved in cofactor binding are marked as X

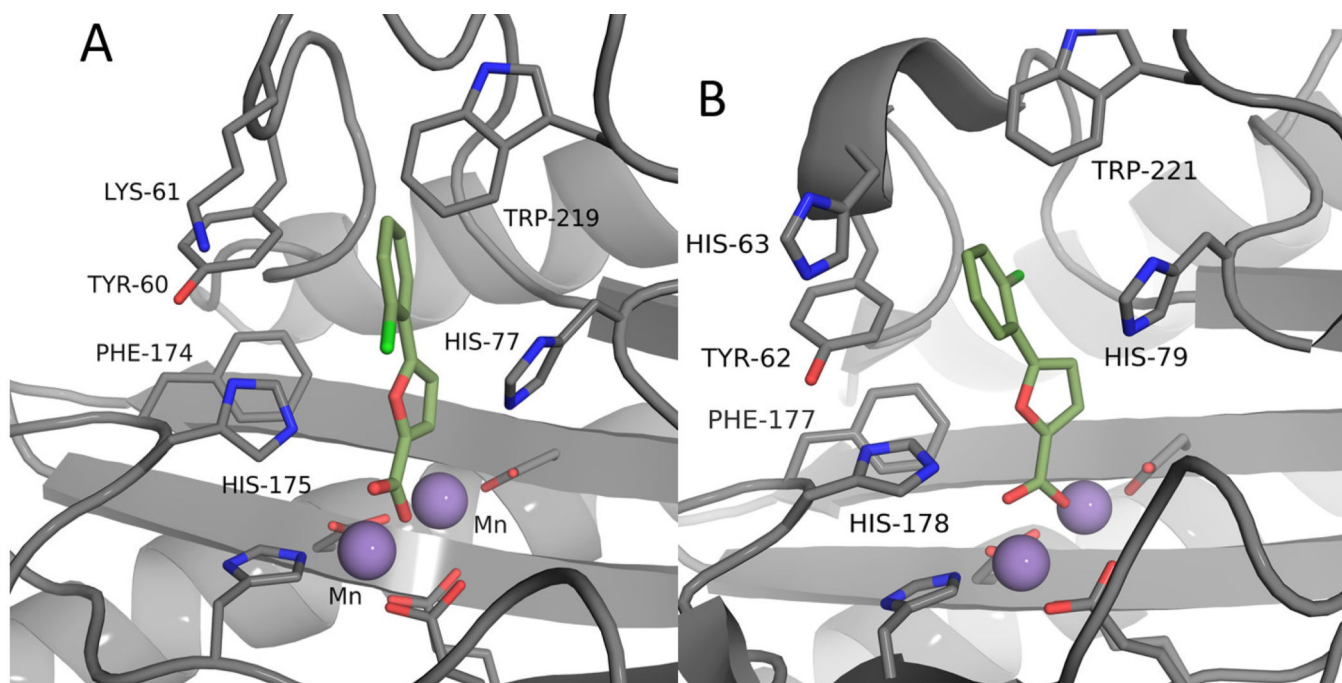


Figure 3. Comparison of docked and observed binding interactions of (**10**). **A:** Docked pose of (**10**) with *RpMetAP* (PDB: 3MX6). **B:** Crystal structure of (**10**) bound to *EcMetAP* (PDB: 1XNZ).¹² Note that residue numbering differs by two between the two MetAP species (Ex: *RpMetAP* Tyr60 and *EcMetAP* Tyr62 are equivalent).

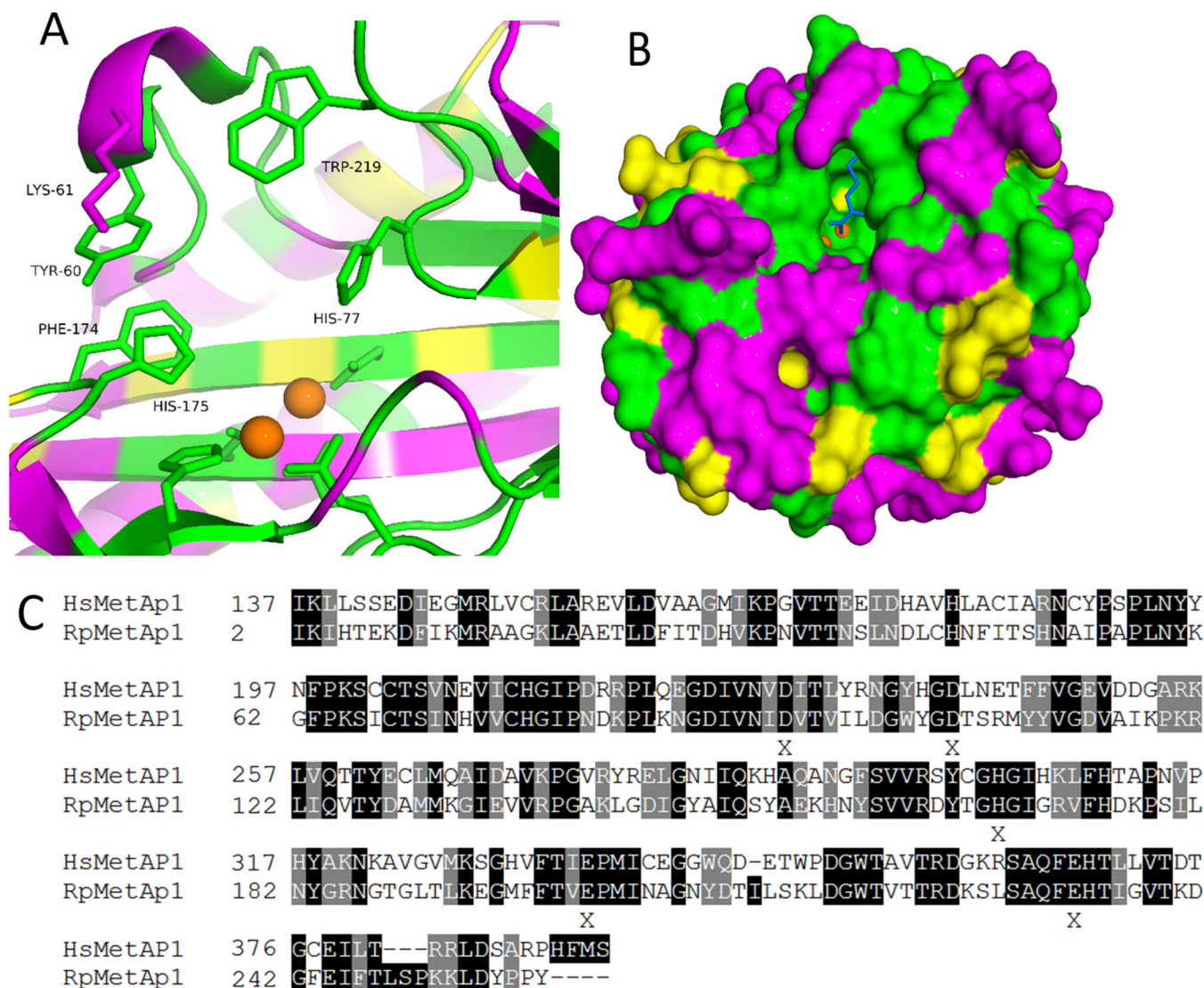


Figure 4. Comparison of *HsMetAP1* and *RpMetAP1* sequences. **A:** Active site of *RpMetAP1* colored according to sequence alignment (green = identity; yellow = similarity; magenta = non-conserved). **B:** Surface diagram of *RpMetAP1* colored according to sequence alignment (green = identity; yellow = similarity; magenta = non-conserved). The blue ligand is a bound methionine and orange spheres are manganese cofactors. **C:** Sequence alignment of *RpMetAP1* (PDB: 3MX6) and *HsMetAP1* (PDB: 2B3K) shaded according to alignment (dark = identity; light = similarity; no-shading = non-conserved). Alignment reveals 43% identity between the proteins. Residues responsible for cofactor binding are marked as X.

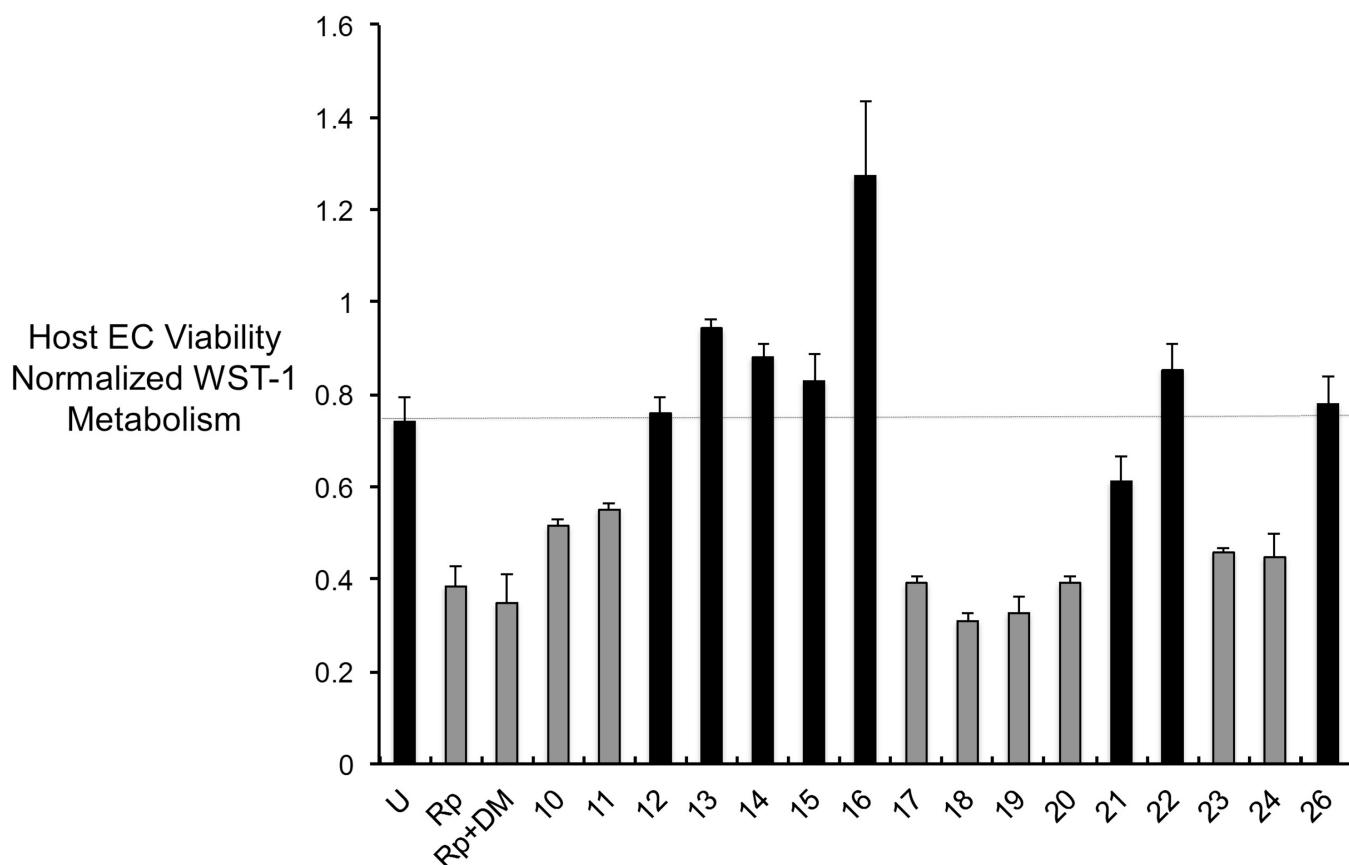


Figure 5.

Effects of *RpMetAP* inhibitors on *R. prowazekii* growth. The loss of infected host ECs viability due to normal *R. prowazekii* growth was used to indirectly assess whether *RpMetAP* inhibitors produced antibacterial effects. The expectation here is that compounds inhibiting rickettsial growth will restore host EC viability to levels comparable to the uninfected control ECs. Host EC viability was measured via WST-1 metabolism (calculated as $A_{450\text{nm}} - A_{660\text{nm}}$ and normalized to media only as background). Solid black bars denote compounds that restored host EC viability to levels comparable to uninfected ECs (denoted by the dashed lines). U = uninfected control ECs; Rp = *R. prowazekii*-infected host ECs; Rp +DM = *R. prowazekii*-infected host ECs treated with the vehicle/solvent control (0.3% DMSO); numbers denote compound identification from Table 6. Infections were performed at a MOI = 100 rickettsiae: 1 host cell. Results represent the average of triplicate infections \pm standard deviation.

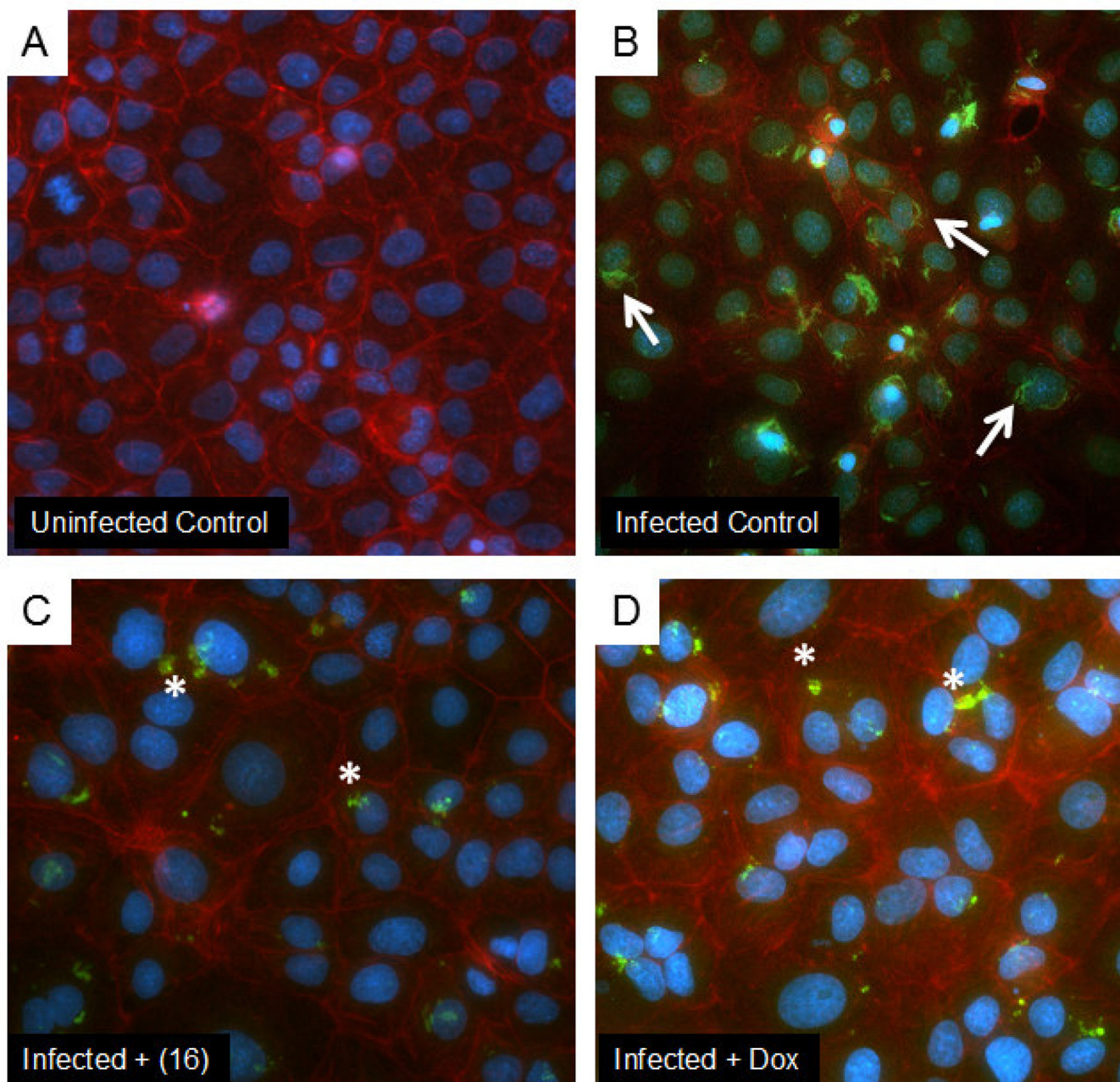


Figure 6. Representative fluorescent micrographs showing effects of *RpMetAP* inhibitor compound (16) compared to a doxycycline control. **Panel A** shows uninfected control ECs. **Panel B** shows ECs infected with *R. prowazekii*. **Panel C** shows the effects of treating *R. prowazekii*-infected ECs with compound (16) (300 μM final concentration). **Panel D** shows the effects of treating *R. prowazekii*-infected ECs with doxycycline (25 μg/mL) as a positive control. Uninfected control cells show very little background antibody staining. The infected control shows infection with many bacilli (white arrows). Treatment with either inhibitor caused bacterial shape changes consistent with condensation and death (white asterisk). Nuclei were stained with Hoescht (blue pseudocolor); actin was stained with Texas Red-labeled

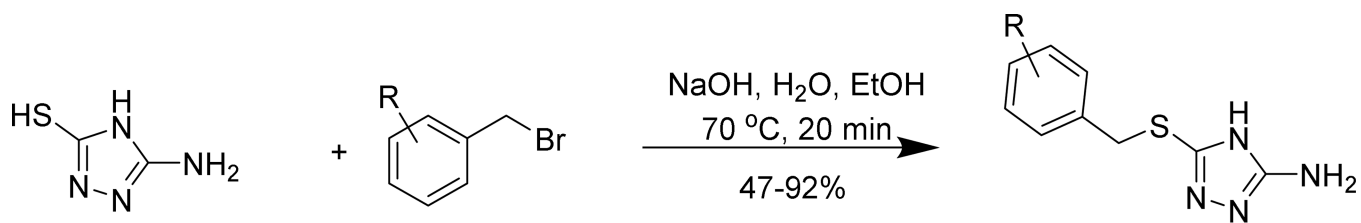
Phalloidin (red pseudocolor); and rickettsiae were stained with a specific antibody conjugated to FITC (green pseudocolor).

Author Manuscript

Author Manuscript

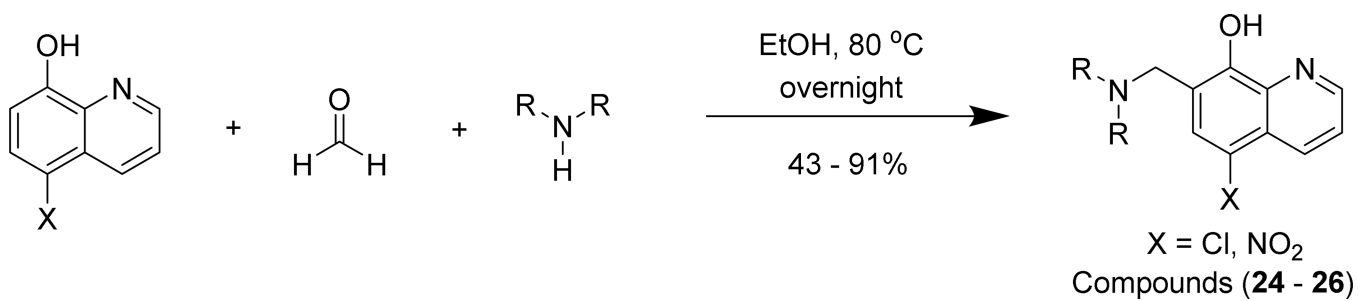
Author Manuscript

Author Manuscript



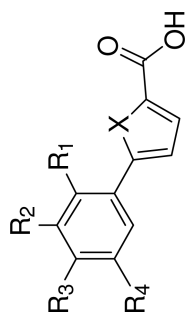
Scheme 1.

Compounds (**12 - 19**)



Scheme 2.

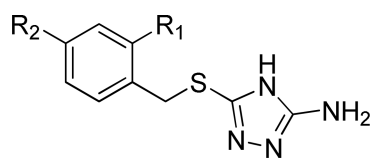
Table 1

Activity of furoic acid species against *RpMetAP1*

Compound	X	R1	R2	R3	R4	IC ₅₀ (μM)	Hill Slope
(1)	S	H	H	H	H	74 ± 7	1.2 ± 0.2
(2)	O	H	NO ₂	H	H	77 ± 4	1.0 ± 0.1
(3)	O	H	CF ₃	H	H	46 ± 2	1.0 ± 0.1
(4)	O	H	H	H	H	37 ± 3	1.0 ± 0.1
(5)	O	H	H	Me	H	57 ± 2	1.0 ± 0.1
(6)	O	CF ₃	H	H	H	0.5 ± 0.1	2.1 ± 0.1
(7)	O	H	H	Br	H	60 ± 5	1.0 ± 0.1
(8)	O	Me	H	H	H	0.9 ± 0.1	1.3 ± 0.1
(9)	O	H	Me	H	H	26 ± 1	1.0 ± 0.1
(10)	O	Cl	H	H	H	0.6 ± 0.1	1.2 ± 0.1
(11)	O	Cl	H	H	Cl	0.6 ± 0.1	0.6 ± 0.1

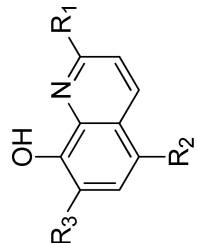
Table 2

Activity of triazole species against RpMetAP1



Compound	R ₁	R ₂	IC ₅₀ (μM)	Hill Slope
(12)	H	H	6.6 ± 1.0	1.1 ± 0.2
(13)	H	Me	23 ± 3	0.9 ± 0.1
(14)	H	F	28 ± 6	1.0 ± 0.2
(15)	Cl	H	15 ± 2	1.2 ± 0.1
(16)	H	Cl	30 ± 2	1.6 ± 0.6
(17)	Cl	Cl	7.7 ± 0.9	1.3 ± 0.3
(18)	H	<i>n</i> Pr	14 ± 1	0.6 ± 0.2
(19)	H	<i>t</i> Bu	14 ± 1	1.5 ± 0.4

Table 3

Activity of quinolinol species against *RpMetAP1*


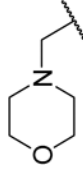
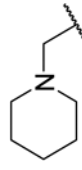
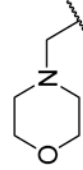
Compound	R ₁	R ₂	R ₃	IC ₅₀ (μM)	Hill Slope
(20)	CH ₃	H	H	1.4 ± 0.1	1.1 ± 0.1
(21)	H	H	H	1.0 ± 0.3	1.2 ± 0.1
(22)	H	Cl	H	0.9 ± 0.1	1.9 ± 0.2
(23)	H	NO ₂	H	1.3 ± 0.7	1.7 ± 0.5
(24)	H	Cl		2.5 ± 0.1	1.5 ± 0.1
(25)	H	NO ₂		73 ± 38	1.2 ± 0.4
(26)	H	NO ₂		16 ± 4	1.0 ± 0.1

Table 4Comparison of binding interactions for (**10**) in crystal and docked structures

Distance ^{a,b}	<i>EcMetAP1</i> Actual	<i>RpMetAP1</i> Docked
Mn(II) Chelation	2.2, 2.3	1.7, 2.1
Mn(II) Coordination	2.0	1.8
π - π Stacking (Tyr62)	4.0	3.1
Hydrophobic (His63)	3.5	6.9 ^c
Hydrophobic (Tyr65)	3.6	3.5
Hydrophobic (His79)	3.6	3.9
Hydrophobic (Phe177)	4.0	3.3
Hydrophobic (His178)	3.3	3.6
Hydrophobic (Trp221)	3.4	3.1
Angle		
Mn(II) – O _L – Mn(II) Angle	107°	155°
(10) Dihedral	41°	18°

^aDistances correspond to closest observed interaction and are reported in Å^bResidue numbering corresponds to *EcMetAP1* (PDB: 1XNZ)¹²^cThis is a non-conserved residue and exists as Lys in *RpMetAP*

Table 5

Comparison of activity (IC) against RpMetAP and HsMetAPs

Compound	RpMetAP1 ^{a,b}	HsMetAP1 ^{c,d}	HsMetAP2 ^{c,e}
(19)	1.4 ± 0.1	>15	>15
(20)	1.0 ± 0.3	>15	2.03 ± 0.3
(21)	0.9 ± 0.1	12.9 ± 1.0	1.27 ± 0.6
(22)	1.3 ± 0.7	>15	0.055 ± 0.02

^aIC₅₀ values in μM^bIC₅₀ values and standard error obtained from nonlinear regression analysis of the average observed activity (in triplicate) versus inhibitor concentration data.^cIn cases where analysis is limited by compound solubility, the minimum estimate of IC₅₀ is provided, Values from Bhat et al.²⁸^dCo(II) cofactors employed in assay^eMn(II) cofactors employed in assay

Table 6

*Rp*MetAP Inhibitory Compounds Tested in EC Culture Infection Model

Compound	MW ^a	Stock (mM) ^b	Test Range (μM) ^c	Growth Inhibition ^d
(10)	222.63	100	300, 30, 3, 0.3	No
(11)	257.07	100	300, 30, 3, 0.3	No
(12)	206.27	100	300, 30, 3, 0.3	Yes
(13)	220.30	100	300, 30, 3, 0.3	Yes
(14)	224.26	100	300, 30, 3, 0.3	Yes
(15)	240.72	100	300, 30, 3, 0.3	Yes
(16)	240.72	100	300, 30, 3, 0.3	Yes
(17)	275.16	100	30, 3, 0.3, 0.03	No
(18)	248.35	100	30, 3, 0.3, 0.03	No
(19)	262.37	100	30, 3, 0.3, 0.03	No
(20)	195.65	100	3, 0.3, 0.03, 0.003	No
(21)	181.62	100	30, 3, 0.3, 0.03	Yes
(22)	245.06	100	30, 3, 0.3, 0.03	Yes
(23)	190.16	100	3, 0.3, 0.03, 0.003	No
(24)	315.20	40	20, 2, 0.2, 0.02	No
(25)	362.25	25	7.5, 0.75, 0.075, 0.0075	No
(26)	325.75	100	3, 0.3, 0.03, 0.003	Yes

^aCompound Molecular Weight in g/mol.

^bStock inhibitor solutions were initially prepared in 100% DMSO to achieve a 100 mM concentration. Compounds that were insoluble at 100 mM were adjusted by addition of DMSO until solubility was achieved.

^cAll compounds were initially tested for toxicity against uninfected ECs. Working concentration test ranges that produced no EC toxicity were selected for further testing against *R. prowazekii*-infected ECs.

^dInhibition of rickettsial growth was determined using the *in vitro* host EC viability assay described in the Experimental Methods section.